

Influence of Si and Ge Microalloying Additions and Plastic Deformation on Precipitation Processes in Al-Cu Based Alloys

Maria Victoria Castro Riglos, Alfredo Tolley

División Física de Metales, Centro Atómico Bariloche, Comisión Nacional de Energía Atómica, San Carlos de Bariloche, Argentina

Email: viquiriglos@gmail.com

How to cite this paper: Castro Riglos, M.V. and Tolley, A. (2018) Influence of Si and Ge Microalloying Additions and Plastic Deformation on Precipitation Processes in Al-Cu Based Alloys. *Journal of Minerals and Materials Characterization and Engineering*, 6, 356-372.

<https://doi.org/10.4236/jmmce.2018.63025>

Received: March 20, 2018

Accepted: May 14, 2018

Published: May 17, 2018

Copyright © 2018 by authors and Scientific Research Publishing Inc. This work is licensed under the Creative Commons Attribution International License (CC BY 4.0).

<http://creativecommons.org/licenses/by/4.0/>



Open Access

Abstract

The combined effect of micro-alloying with Si and Ge and/or plastic deformation prior to ageing at 160°C on age hardening has been studied in an Al-2 at% Cu alloy. The results obtained indicate that the hardness response is faster and the peak hardness is higher when plastic deformation and micro-alloying are applied together than performing each procedure individually. Different amounts of deformation, ranging from 0% to 30% have been utilized. An optimum deformation degree for the hardening response has been established around 8% for the Al-Cu-Si-Ge alloy. Characterization by transmission electron microscopy (TEM) shows that the peak hardness is due to a complex microstructure that contained θ'' disc shaped precipitates, rod-shaped Si-Ge precipitates and θ' plates that were heterogeneously nucleated on the Si-Ge particles. Pre-deformation has been found to stimulate the growth of the θ' plates due to enhanced diffusion along dislocation cores. Increasing deformation reduces the influence of the Si-Ge precipitates on heterogeneous nucleation, leading to reduced peak hardness and faster over-ageing.

Keywords

Al-Cu Based Alloys, Precipitation, Microstructure, Hardness, Transmission Electron Microscopy

1. Introduction

The Al-Cu system has been extensively investigated as a model system for precipitation hardening. In fact, the phenomenon of precipitation hardening has been first discovered in an Al-Cu based alloy [1]. In order to improve the hardening

evolution in heat treatable alloys, several methods have been devised. One method involves the addition of small amounts of alloying elements, known as micro-alloying elements [2]-[15]. Another method is to apply a plastic deformation before artificial ageing takes place [4] [16] [17]. Both methods result in faster hardening kinetics and higher hardness values by modifying the precipitation process.

In Al-Cu based alloys, different kinds of micro-alloying additions have been studied. Trace additions of Sn, Cd and In to Al-Cu have been shown to enhance the hardening rate and to increase peak hardness [2] [4] [5]. In ternary Al-Cu-Mg alloys, the effects of minor Ag additions have been demonstrated to stimulate the precipitation of different metastable phases, depending on the Cu:Mg ratio [6]-[12]. The addition of Si and Ge in equal proportions has also been proved to increase the hardening rate during artificial ageing, together with an increase in peak hardness [14] [15]. It has been observed that diamond cubic Si-Ge precipitates provide nucleation sites for metastable θ' phase, leading to a high density of such precipitates at peak hardness.

Plastic deformation prior to artificial ageing has been able to increase peak hardness in binary Al-Cu alloys as well [4]. In this case, the increase in hardening rate has been related to faster diffusion paths along the dislocations introduced by plastic deformation. Furthermore, dislocations also serve as heterogeneous nucleation sites for precipitates, thus enhancing the nucleation rate [4]. In the commercial 2024 alloy, plastic deformation prior to artificial ageing has been found to increase the hardening rate and peak hardness. Microstructural characterization has shown that dislocations provide nucleation sites for the S phase, resulting in a homogeneous distribution of S phase precipitates [16] [17].

However, in Al-Cu alloys, the combination of microalloying additions of Cd and plastic deformation prior to artificial ageing has been found to produce worse results than for each method applied individually [18].

On the contrary, in Al-Cu with minor additions of Si and Ge, the combination of microalloying and plastic deformation prior to artificial ageing at 190°C led to an acceleration of the ageing response [19].

The main goal of the present study is to further analyze the combined effects of microalloying with Si and Ge and plastic deformation in an Al-2 at% Cu alloy. For this purpose, different degrees of deformation prior to artificial ageing at 160°C have been applied. The hardness evolution during artificial ageing is studied and microstructural characterization by means of transmission electron microscopy (TEM) is also carried out after specific ageing times. In addition, to help understanding the processes involved, the simpler related systems (Al-Cu and Al-Si-Ge) are analyzed.

2. Experimental

Alloys with the following nominal compositions were melted in an arc furnace: Al-0.5Si-0.5Ge, Al-2Cu, Al-2Cu-0.5Si-0.5Ge (at%). All of these alloys were ho-

mogenized at 520°C under an Argon atmosphere.

Three specimens (diameter = 6 mm and length = 2 cm) from each alloy were machined. Two cylinders were subjected to either 8% or 15% deformation in compression, using an INSTRON 5563 Mechanical Testing Machine. The remaining cylinder was not deformed. Slices that were 1 mm in thickness were cut from each cylinder and were artificially aged at 160°C for different ageing times, t_a . For the Al-Cu-Si-Ge alloy a fourth specimen that had been pre-deformed to 30% by cold rolling was also studied.

The evolution of Vickers Hardness (H_v) as a function of t_a was obtained for each degree of deformation; a Mitutoyo Hardness Testing Machine with a load of 100 g was used to make the measurements.

Samples for TEM characterization were prepared by mechanical grinding followed by double jet electropolishing with an electrolyte based on Methanol and a mixture of H₂SO₄, HF and Glycerol. The microstructure was analyzed after specific ageing conditions that were of interest using a Philips CM200 UT microscope with a LaB₆ filament and a FEI Tecnai F20 microscope with a Schottky field emission gun, both operated at 200 KeV. In order to determine precipitate densities, the local thickness was measured using convergent-beam electron diffraction (CBED) in a two-beam condition with $g = 200_{Al}$ as reported by Kelly [20].

3. Results

3.1. Hardness Measurements

Hardness evolution as a function of ageing time is displayed in **Figure 1** where the behavior of the pre-deformed and non-deformed specimens is compared for each alloy.

For the ternary Al-Si-Ge alloy (**Figure 1(a)**) the hardness evolution curve has been uniformly shifted for all ageing times to higher values as a result of pre-deformation. The shift for 15% deformation was around two or three times larger than the shift observed for a deformation of 8%. The ageing time at which peak hardness occurred was 20 h for all cases, independent of the degree of pre-deformation.

For the binary Al-Cu alloy (**Figure 1(b)**), the annealing time required to reach the peak aged (PA) condition was significantly reduced. In the case of the undeformed alloy the maximum was observed for $t_a \sim 60$ h and it remained constant for longer ageing times while for the pre-deformed alloys (either 8% or 15%) the peak was achieved after only 20 h ageing. However, the peak hardness was unaffected by pre-deformation.

Figure 1(c) shows the combined effect of microalloying and pre-deformation on Al-Cu.

The non-deformed Al-Cu alloy with minor additions of Si and Ge reached peak hardness after 20 h ageing, a considerably shorter time than for the binary alloy; in addition the peak hardness ($H_v = 170$) was considerably higher. After

8% pre-deformation, hardness increased faster during the early stages of ageing and reached an even higher hardness ($H_v = 190$) at the same peak ageing time of 20 h.

The main results extracted from **Figure 1** (*i.e.* PA hardness, H_v , and ageing time, t_a) are summarized in **Table 1** for each alloy and for each pre-deformation degree $\leq 15\%$. The results for the 30% pre-deformed Al-Cu-Si-Ge alloy ($H_v = 160 \pm 5$ and $t_a = 3$ h) were not included in **Table 1** as they were almost coincident with those from the 15% pre-deformed Al-Cu-Si-Ge specimen.

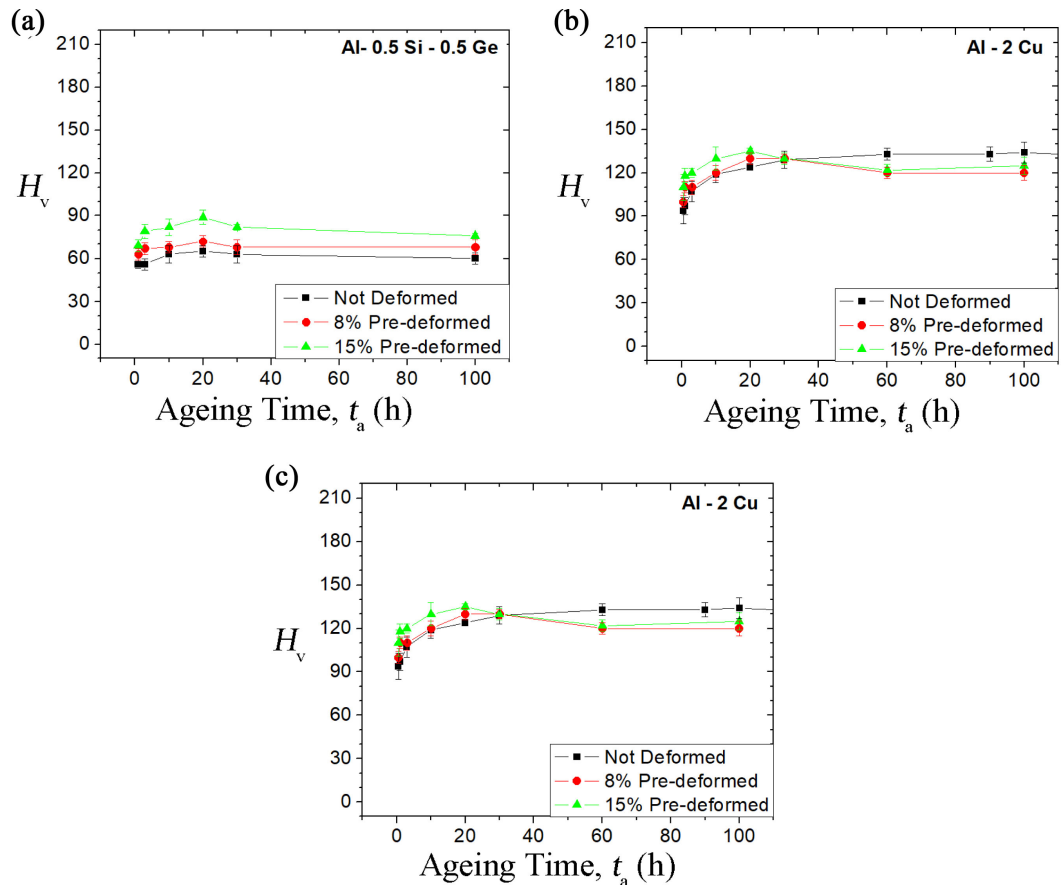


Figure 1. Hardness evolution as a function of ageing time (t_a) with different degrees of pre-deformation for each alloy system: (a) Al-0.5Si-0.5Ge, (b) Al-2Cu, (c) Al-2Cu-0.5Si-0.5Ge (in at%). All heat treatments were performed at 160°C .

Table 1. PA hardness and ageing time for non-deformed and pre-deformed specimens of each alloy.

Alloy System	PA	No Def	8% Def	15% Def
Al-Si-Ge	H_v	65 ± 4	72 ± 4	89 ± 5
	t_a (h)	20	20	20
Al-Cu	H_v	134 ± 7	130 ± 4	135 ± 2
	t_a (h)	100	20	20
Al-Cu-Si-Ge	H_v	170 ± 10	190 ± 10	170 ± 10
	t_a (h)	20	20	3

After 15% pre-deformation, the hardening response was even faster, reaching peak hardness at an ageing time of 3 h, but the peak hardness was the same as that obtained in the non-deformed condition. Increasing the pre-deformation to a degree of 30% resulted in an acceleration of the overageing stage and a reduction of the peak hardness. These results suggest that the optimum pre-deformation that produces maximum peak hardness is around 8% or could be even lower.

3.2. Microstructural Characterization

3.2.1. PA Microstructure: Al-Cu and Al-Cu-Si-Ge

In order to understand the observed hardness behavior, the microstructure of the Al-Cu and Al-Cu-Si-Ge alloys after certain ageing times at 160°C, with and without pre-deformation of 8% has been investigated with TEM observations.

Figure 2 shows dark field (DF) images of the Al-Cu alloy in the undeformed and after 8% pre-deformation conditions, after 20 h ageing. For the 8% pre-deformed condition this corresponds to the PA condition.

Dark field images in **Figure 2** have been obtained in 2-beam diffraction condition with the reflection $\mathbf{g} = 200_{\text{Al}}$, its direction is indicated in the bottom-left corner in each micrograph.

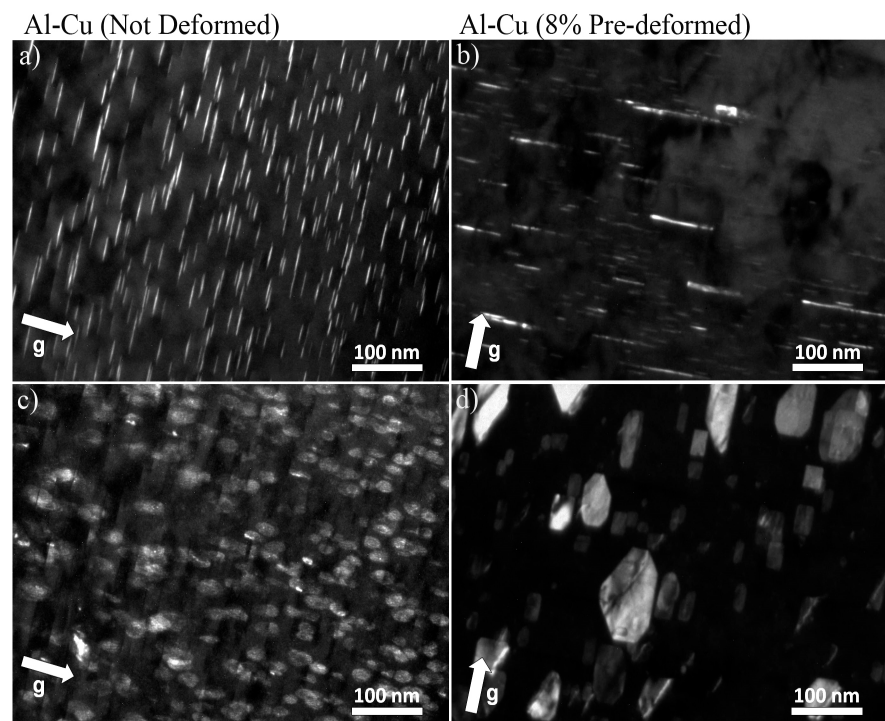


Figure 2. DF images in Al-Cu, $t_a = 20$ h: with no deformation (left column) and with 8% pre-deformation (right column). All images were acquired in two-beam condition with the $\mathbf{g} = (200)_{\text{Al}}$ reflection (described by a thick arrow in the left bottom corner within each image), close to $\text{ZA} = [011]_{\text{Al}}$. (a) (b) Edge-on θ' or θ'' precipitates (only one of the three variants), obtained from weak reflections at $\sim(1/2)\cdot\mathbf{g}$; (c) (d) Inclined θ'' precipitates and also some θ' precipitates in **Figure 2(d)** (one of the two other variants) are highlighted by tilting slightly away from the $\text{ZA} = [011]_{\text{Al}}$ and using the reflections from $(112) \theta'' / \theta'$ planes.

The specimen was oriented close to the $[011]_{\text{Al}}$ matrix Zone Axis (ZA). In **Figure 2(a)** and **Figure 2(b)** weak reflections about midway between the transmitted (000) and the diffracted (200_{Al}) beams were used to highlight one of the three variants of the θ' or θ'' precipitates. In this condition the imaged plate shape precipitates were parallel to the electron beam so they are displayed “edge-on”. In **Figure 2(c)** and **Figure 2(d)** dark field images from one of the two other variants of the θ' or θ'' precipitates, inclined to the beam direction were obtained using (112) θ'' / θ' type reflections, by tilting slightly away from the $[011]_{\text{Al}}$ matrix Zone Axis (ZA). While for the non-deformed condition only θ'' precipitates were observed (**Figure 2(a)** and **Figure 2(c)**), in the 8% pre-deformed condition larger θ' phase precipitates were observed together with a high density of smaller θ'' phase precipitates. In **Figure 2(b)** the edge-on θ'' precipitates are shorter and thinner than the θ' precipitates. In **Figure 2(d)** the inclined θ'' precipitates show weaker contrast than the larger θ' phase precipitates.

Results of precipitate size and density measured on micrographs like those shown in **Figure 2** are summarized in **Table 2**. The lengths (ℓ) correspond to the average diameter of the disc-shaped θ'' or plate-shaped θ' precipitates, respectively. The average lengths are reported accompanied by their error ($\Delta\ell$) and, in brackets, by their Standard Deviation (SD) to have an idea of the precipitate sizes dispersion. The error, $\Delta\ell$, was considered to be the SD divided by \sqrt{N} , where N is the number of measured precipitates.

To obtain the precipitate densities (ρ) the local thickness was measured using CBED patterns in a two-beam condition with $\mathbf{g} = 200_{\text{Al}}$ as reported by Kelly *et al.* [20].

The density of the θ' precipitates in the pre-deformed specimen was estimated from the proportion between the θ'' and the θ' precipitates observed in pictures like those in **Figure 2(b)** and **Figure 2(d)**. The amount of the θ' precipitates was accounted to be around 15% of the amount of the θ'' precipitates.

For the Al-Cu-Si-Ge alloy, DF images in **Figure 3** were obtained in two beam condition with $\mathbf{g} = 200_{\text{Al}}$ and with the sample oriented close to $\text{ZA} = [011]_{\text{Al}}$ in the same way as those DF images presented in **Figure 2** for the Al-Cu alloy. In **Figure 3(a)** and **Figure 3(b)**, DF images show edge-on θ' and θ'' precipitates

Table 2. Effect of pre-deformation on the diameter and density of θ'' and θ' precipitates for the Al-Cu system after 20 h ageing at 160°C. The obtained average lengths (ℓ) and the densities (ρ) for each precipitate type are shown. The lengths are reported together with their error and, in brackets, their standard deviation.

Al-Cu		No Def	8% Def
θ''	$\ell \pm \Delta\ell$ (nm)	16 ± 0.2 (5)	16 ± 0.5 (5)
	$\rho \pm \Delta\rho$ ($\text{nm}^{-3} \times 10^{-5}$)	4.5 ± 0.4	3.3 ± 0.3
θ'	$\ell \pm \Delta\ell$ (nm)	-	40 ± 2 (20)
	ρ ($\text{nm}^{-3} \times 10^{-6}$)	-	~ 5

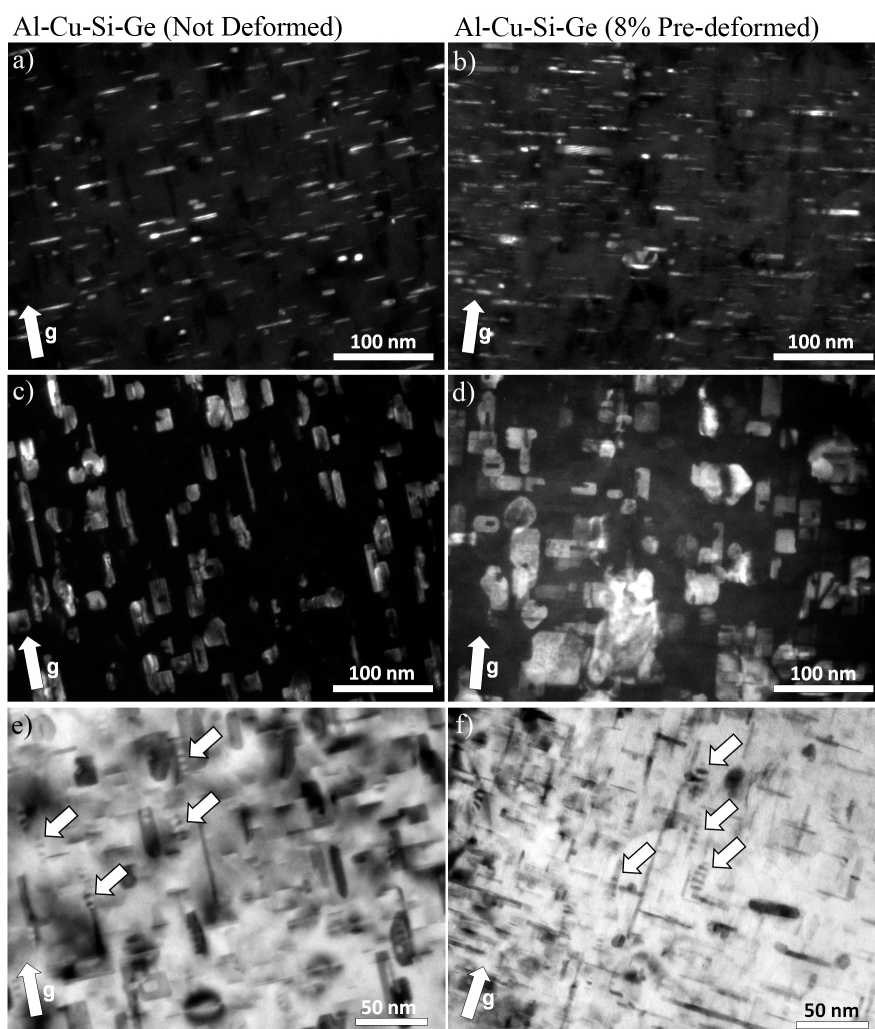


Figure 3. Microstructure in Al-Cu-Si-Ge without pre-deformation (left) and after 8% pre-deformation (right), in PA ($t_a = 20$ h). All images were obtained in 2-beam condition with $g = (200)_{Al}$ near to the $[011]_{Al}$ Zone Axis. Vector g is indicated in the bottom left corner of every image. (a) (b) Edge-on θ' precipitates, highlighted by selecting the weak reflection placed at $\sim(1/2)g$ (only one of the three variants); (c) (d) Inclined precipitates (one of the two other variants) are highlighted by tilting slightly away from the ZA = $[011]_{Al}$ and using a reflection from $(112) \theta'$ planes; (e) (f) BF images showing bar type Si-Ge precipitates with fringed Moirée pattern (one of three variants). White short arrows are pointing at some of these Si-Ge bar precipitates.

that are highlighted using the $(002) \theta'$ or $(002) \theta''$ reflections at $\sim(1/2)g$, while in **Figure 3(c)** and **Figure 3(d)** only inclined θ' precipitates are observed by selecting the $(112) \theta'$ reflection. It's worth noting (as well as for Fig. 2d) that although both θ' and θ'' precipitates were present, the contrast from θ'' was very weak and these precipitates were not easily seen in this condition.

Si-Ge precipitates in the Al-Cu-Si-Ge alloy formed with a rod-shaped morphology oriented parallel to the $\langle 001 \rangle$ matrix directions, with the $[001]_{Al} || [112]_{Si-Ge}$, $[100]_{Al} || [1-10]_{Si-Ge}$, and $[010]_{Al} || [-1-11]_{Si-Ge}$ orientation relationship [15]. **Figure 3(e)** and **Figure 3(f)** show bright field (BF) images ob-

tained at the Bragg condition with the matrix reciprocal lattice vector $\mathbf{g} = 200_{\text{Al}}$, in which the Si-Ge rods show a characteristic Moirée fringe contrast due to the very similar lattice spacings of the nearly coincident $\mathbf{g} = 200_{\text{Al}}$ and $\mathbf{g} = -220_{\text{Si-Ge}}$. A few Si-Ge precipitates are indicated with white and short arrows in **Figure 3(e)** (non-deformed specimen) and **Figure 3(f)** (8% pre-deformed specimen) BF images.

Measured precipitate sizes and densities of the θ'' , θ' and Si-Ge precipitates in the Al-Cu-Si-Ge alloy (with and without pre-deformation) in peak aged condition are given in **Table 3**. The length (ℓ) of the θ' precipitates corresponds to their average projected plate diameter, determined in 2-beam condition with the 200 reflection strongly excited (**Figure 3(a)** and **Figure 3(b)**). In this condition, the θ'' phase precipitates were differentiated from those of the θ' phase due to their much smaller thickness. In the same way as for the **Table 2**, the average lengths in **Table 3** are reported accompanied by their error and, in brackets, by their Standard Deviation. Considering that a large amount of precipitates was measured (usually between 100 and 400 precipitates in each case), the main source for error in ρ was attributed to the error in the local foil thickness determination. Thus, the uncertainty in all the measured density values ($\Delta\rho$) was estimated to be 10%.

3.2.2. Underaged Microstructure in Al-Cu-Si-Ge

To analyze why differences in peak aged microstructure were generated between the un-deformed and the 8% pre-deformed Al-Cu-Si-Ge, specimens in the underaged condition were also studied. **Figure 4(a)** and **Figure 4(b)** show high resolution (HR) images to illustrate the microstructure at a very early stage of ageing ($t_a = 3$ h), for both non-deformed and pre-deformed samples. In both cases, a very high density of θ'' precipitates was observed, together with occasional Si-Ge and θ' precipitates. For the non-deformed specimen, **Figure 4(a)** displays a Si-Ge precipitate imaged “end-on”, that is, with the long direction of the rod parallel to the electron beam. A detailed view of this same Si-Ge precipitate is shown in **Figure 4(c)**. In addition, a detailed view of a θ' “edge-on” precipitate can be seen in **Figure 4(e)**.

Table 3. Effect of pre-deformation on the length and density of θ'' and θ' precipitates for Al-Cu-Si-Ge in PA condition ($t_a = 20$ h). The obtained average lengths (ℓ) and the densities (ρ) for each precipitate type are shown. The lengths are reported together with their error and, in brackets, their Standard Deviation.

Al-Cu		No Def	8% Def
θ''	$\ell \pm \Delta \ell$ (nm)	12 ± 0.3 (4)	12 ± 0.2 (4)
	$\rho \pm \Delta \rho$ ($\text{nm}^{-3} \times 10^{-5}$)	9 ± 0.9	9 ± 0.9
θ'	$\ell \pm \Delta \ell$ (nm)	20 ± 0.3 (7)	28 ± 0.4 (10)
	$\rho \pm \Delta \rho$ ($\text{nm}^{-3} \times 10^{-5}$)	6.8 ± 0.7	6.4 ± 0.6
Si-Ge	$\ell \pm \Delta \ell$ (nm)	20 ± 1 (4)	21 ± 1 (6)
	$P \pm \Delta P$ ($\text{nm}^{-3} \times 10^{-5}$)	4 ± 0.4	3.7 ± 0.4

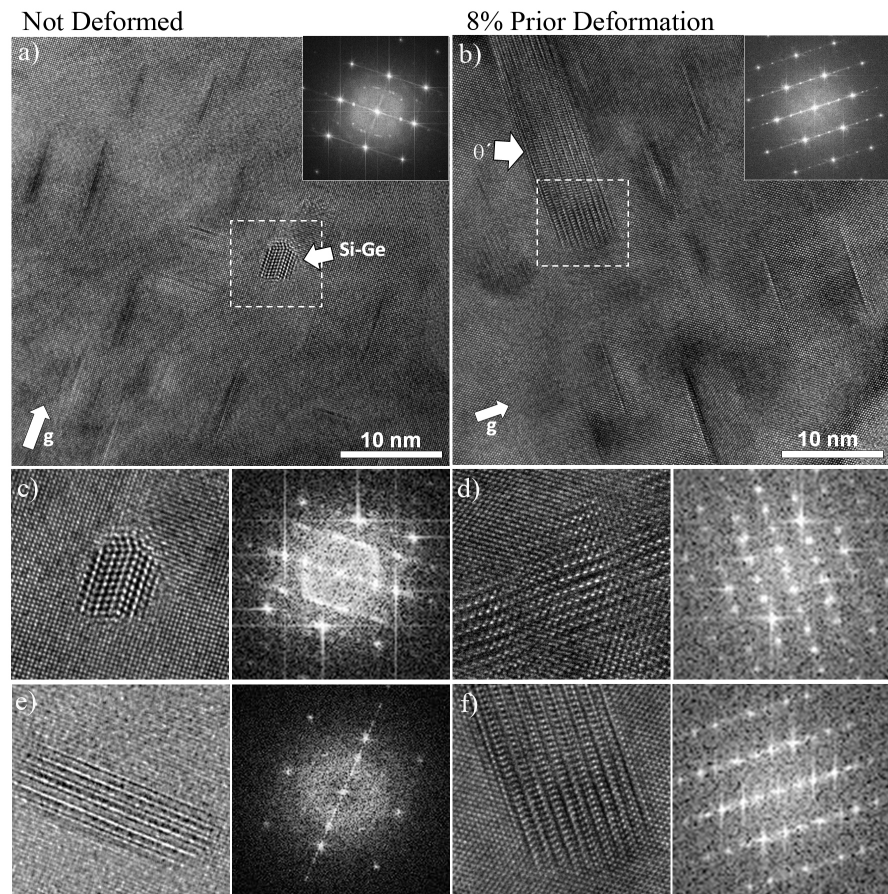


Figure 4. HR images of Al-Cu-Si-Ge alloy without pre-deformation (left) and after 8% deformed (right), in an early underaged condition, $t_a = 3$ h. Images in the un-deformed alloy were obtained with the electron beam parallel to $ZA = [001]_{Al}$ while in the case of the pre-deformed specimen the electron beam was oriented parallel to $[011]_{Al}$ Zone Axis. (a) (b) General view, FFTs are calculated over the whole images and displayed within the top right corner. (c) (d) Detailed view of Si-Ge precipitates: the precipitate in (c) is oriented “end on” and is the same one enclosed in dotted lines in (a). The precipitate in (d) has its longest dimension lying parallel to $[100]_{Al}$ direction thus Moirée contrast can be observed. (e) (f) Detailed view of θ' precipitates imaged “edge on”, the precipitate in (f) corresponds to the area enclosed in dotted lines in (b). All the sub-images in (c)-(f) have a width of 10 nm and are displayed together with their FFT (these FFTs are calculated only in the small region where the precipitate is shown). Each FFT has a width of 18.5 nm^{-1} .

For the 8% pre-deformed specimen, a detailed view of a Si-Ge precipitate lying along the $[100]_{Al}$ direction is presented in **Figure 4(d)**, displaying the characteristic Moirée contrast. **Figure 4(f)** shows an area of **Figure 4(b)** at higher magnification, containing a detail of a θ' precipitate oriented “edge on”.

It is important to mention that in **Figure 4(a)**, **Figure 4(c)** and **Figure 4(e)** the specimen is oriented with the $[001]_{Al}$ zone axis parallel to the electron beam. Thus, 2 variants of θ'' precipitates can be observed edge-on. In **Figure 4(b)**, **Figure 4(d)** and **Figure 4(f)** the electron beam has been parallel to the $[011]_{Al}$ zone axis, so only 1 variant of the θ'' (or θ') precipitates is imaged

“edge-on”. The insets in **Figure 4(a)** & **Figure 4(b)** show the Fast Fourier Transform (FFT) calculated over the whole image. The strongest spots in these FFTs correspond to the Al matrix planes while the weaker ones belong to the secondary phases (θ'' , Si-Ge and θ'). These weak spots are better observed when the FFT is calculated for each particular precipitate (FFT in **Figures 4(c)-(f)**).

At this short ageing time ($t_a = 3$ h), precipitates from θ' phase are rarely observed in the non-deformed specimen (**Figure 4(e)**) although they are often observed after pre-deformation. Furthermore, in this latter case θ' precipitates appeared more developed (**Figure 4(b)**, **Figure 4(f)**) and more frequently, but not always, attached to a Si-Ge bar.

After a longer ageing time ($t_a = 10$ h), θ' precipitates are abundant in both un-deformed and deformed conditions. The DF images shown in **Figure 5(a)** and **Figure 5(b)**, have been obtained in 2-beam condition with the $g = 200_{\text{Al}}$ reflection from Al matrix at the Bragg condition, being close to the $ZA = [011]_{\text{Al}}$. A reflection from (112) θ' planes has been used to highlight θ' precipitates inclined with respect to the electron beam. Some notches can be observed in θ' plates (indicated with yellow arrows) that evidence heterogeneous nucleation of this θ' phase on previously formed Si-Ge precipitates [14]. It can be clearly seen that θ' precipitates are more developed in the pre-deformed sample.

3.2.3. Higher Deformation Degrees (15% Def.) and the Effect on Microstructure

Figure 6 shows the microstructural evolution in Al-Cu-Si-Ge after 15% pre-deformation, for three different ageing conditions: underaging ($t_a = 1$ h), peak aged ($t_a = 3$ h) and overaged ($t_a = 100$ h).

The HR images were obtained in 2-beam condition using (200) reflections

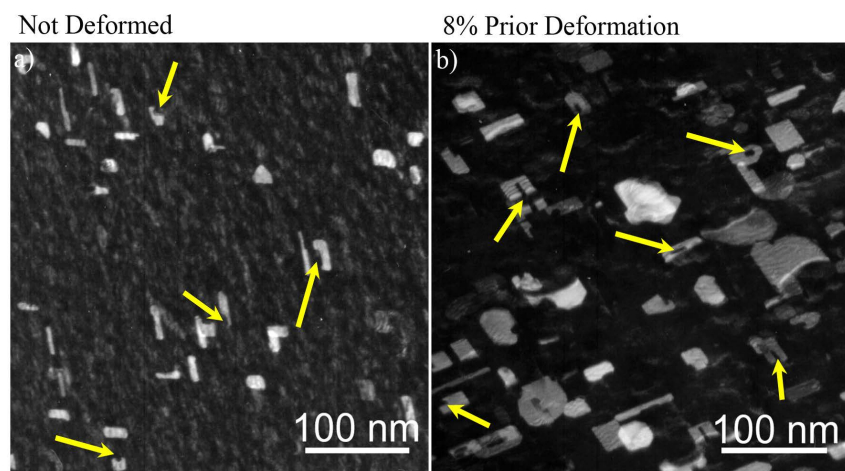


Figure 5. Microstructure of Al-Cu-Si-Ge alloy in a slightly underaged condition, $t_a = 10$ h: (a) without pre-deformation, (b) after 8% pre-deformation. In both cases DF imaging was performed in a two-beam condition with $(200)_{\text{Al}}$ reflection close to $ZA = [011]_{\text{Al}}$. The inclined θ' plates are highlighted using a reflection from (112) θ' planes. The yellow arrows are pointing out some notches on the θ' precipitates which indicate heterogeneous precipitation of the θ' phase on the previously formed Si-Ge precipitates.

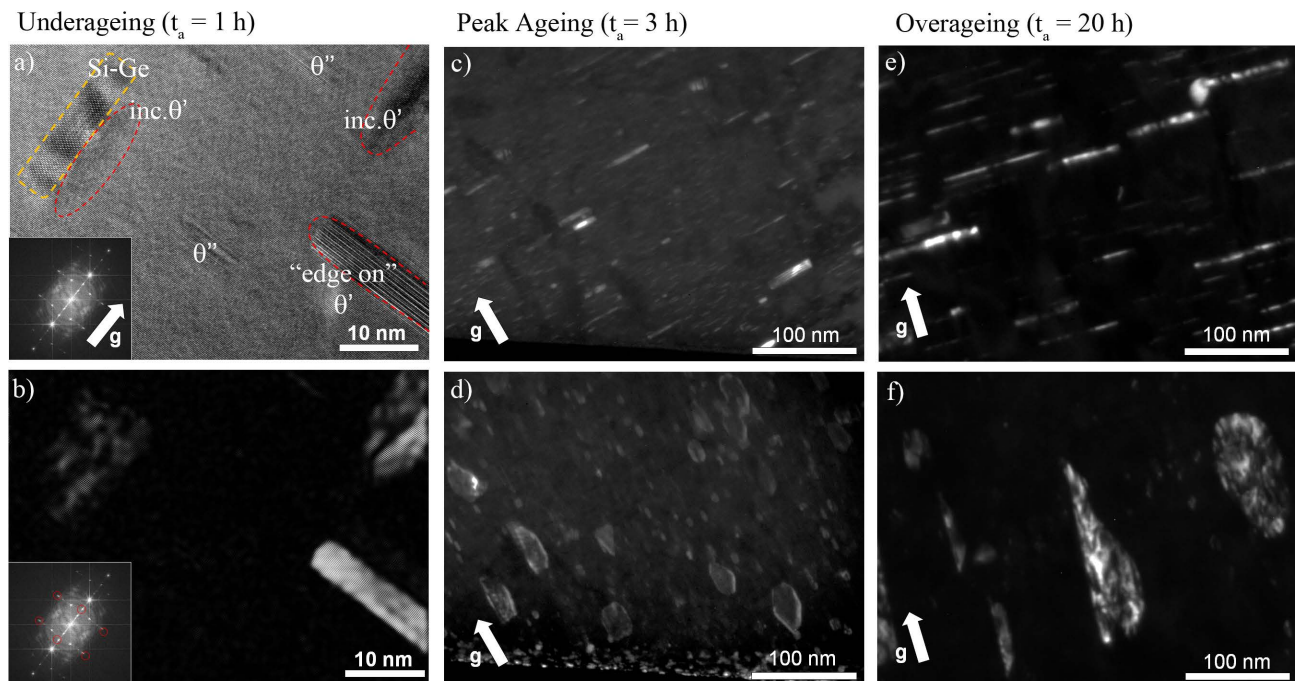


Figure 6. Microstructure evolution in the Al-Cu-Si-Ge alloy after 15% pre-deformation. (a) (b) Underaging ($t_a = 1$ h): (a) Shows a HR image where a Si-Ge precipitate is observed (orange dotted line) associated to an inclined θ' precipitate (red dotted line). Two other θ' precipitates and some small “edge-on” θ'' precipitates are observed. In (b), the IFFT highlights every θ' precipitate shown in a) as it has been calculated by using the spots that are circled within the FFT (inset). ((c), (d)) PA ($t_a = 3$ h): many small θ'' precipitates are observed together with some large θ' precipitates. (e) (f) Overaging ($t_a = 100$ h): a reduced amount of θ'' precipitates and some large θ' precipitates are observed. For DF images in (c) and (e) the “edge-on” θ''/θ' precipitates are highlighted by selecting the reflection at $\sim(1/2).g$ while within d) and (f) the inclined θ''/θ' precipitates are highlighted using the reflection $(112)\theta'$. All images are obtained in 2-beam condition with $g = 200_{Al}$, close to $ZA = [011]_{Al}$.

from the Al matrix that were close to $[011]_{Al}$ zone axis.

In the under-aged condition (**Figure 6(a)**), HR imaging allows the observation of a Si-Ge precipitate (enclosed by an orange dotted line) which is associated to an inclined precipitate from θ' phase (inside a red dotted line). Two other θ' precipitates which are not attached to Si-Ge precipitates are shown inside red dotted lines, one of them (perpendicularly oriented with respect to the Si-Ge rod) is oriented “edge-on”. Moreover, some smaller “edge-on” θ'' precipitates are seen parallel to this θ' plate. In **Figure 6(b)**, every θ' precipitate in **Figure 6(a)** is highlighted by Fourier filtering. The image was obtained by calculating the Inverse Fast Fourier Transform (IFFT), using the spots circled in the corresponding FFT (**Figure 6(b)** inset).

Figure 6(c) and **Figure 6(d)** are DF images showing the peak aged microstructure ($t_a = 3$ h) where many small θ'' precipitates are observed together with some large θ' precipitates. For the overaged condition ($t_a = 100$ h), **Figure 6(e)** and **Figure 6(f)** show a reduced amount of θ'' precipitates and some very large, sparsely distributed θ' precipitates.

In **Figure 6(c)** and **Figure 6(e)** the precipitates are observed “edge-on” because they are highlighted using the reflection at $\sim(1/2).g$, while in **Figure 6(d)**

and **Figure 6(f)** the precipitates are inclined with respect to the electron beam and they are highlighted by selecting the reflection from the (112) θ'' / θ' planes.

4. Discussion

For the Al-Si-Ge system the hardness evolution after pre-deformation shows a uniform shift towards higher values for all ageing times. This shift is larger for higher degrees of deformation. However, this shift is not significant. The peak hardness after 15% pre-deformation barely reaches the value of the initial hardness in the Al-Cu alloy at very short ageing times (**Figure 1(a)** and **Figure 1(b)**). The fact that the same shift is obtained for all ageing times indicates that this shift can be attributed to work hardening and that the dislocations introduced by pre-deformation did not alter the nucleation and growth processes. It also suggests that the additional dislocations introduced by the previous deformation did not provide additional nucleation sites for the precipitation process, since this would alter the precipitation kinetics and thus modify the hardness evolution.

The main effect of pre-deformation in the Al-Cu system is a significant reduction in the ageing time to reach peak hardness, while the maximum H_v value is unaffected. The TEM observations show that pre-deformation enhances the precipitation of the θ' phase, as previously reported by Silcock [4]. Whereas without pre-deformation the microstructure at peak hardness in Al-Cu ($t_a = 100$ h) contained only θ'' precipitates, after pre-deformation the peak hardness microstructure contained sparsely distributed θ' precipitates among a dense distribution of θ'' precipitates.

Microalloying additions of Si and Ge to Al-Cu exhibit a marked increase in peak hardness values compared to the binary Al-Cu alloy, confirming previously reported results for artificial ageing at 190°C [14] [15] [19]. For treatment at 160°C, the time to reach peak ageing has been longer and the maximum hardness obtained is higher when compared to the values measured after ageing at 190°C (20 h as compared to 3 h, and $H_v = 170$ as compared to $H_v = 158$ for ageing at 160°C and 190°C, respectively). This is the expected behavior for precipitation processes and can be explained by an increased undercooling at 160°C, that produces a higher density of precipitates due to a larger driving force, but slower precipitation kinetics due to the lower temperature.

TEM characterization evidences that at 160°C the microstructure in the peak aged condition is complex and included small disc shaped θ'' precipitates parallel to the {100} matrix planes, rod-shaped Si-Ge precipitates, parallel to the $\langle 100 \rangle$ matrix directions and plate shaped θ' precipitates parallel to the {100} matrix planes. The rod-shaped morphology of the Si-Ge precipitates in the aluminum matrix is characteristic of Cu containing alloys and differs from that of the ternary Al-Si-Ge alloy where equiaxed precipitates are dominant, as previously described by Mitlin *et al.* [15] and by Mukhopadhyay [21].

These Si-Ge precipitates are effective nucleation sites for heterogeneous preci-

pitiation of θ' phase, thus reducing the ageing time to reach peak hardness and achieving a higher hardness. However, the microstructure observed at peak ageing at 160°C differs from that observed at peak ageing when aging is performed at 190°C [15], where only Si-Ge and θ' precipitates are observed, but no θ'' precipitates. At this ageing temperature (190°C), θ'' precipitates are formed during the early stages of ageing but dissolved completely in favor of the θ' precipitates once the peak hardness ageing time is reached. The high density of θ'' precipitates observed in the peak aged condition at 160°C suggests that such precipitates contribute significantly to peak hardness. This conclusion is supported by comparing the precipitate densities measured at peak ageing in 8% pre-deformed material after aging at 160°C with those reported in an alloy of similar composition but aged at 190°C [19]. After aging at 190°C, the microstructure contains only Si-Ge precipitates and θ' plates with similar densities to those observed in the present work, but peak hardness is significantly lower ($H_v = 160$) than after ageing at 160°C ($H_v = 190$). The difference in peak hardness can then be attributed to the additional θ'' precipitates observed after ageing at 160°C.

An important result in this work is that for the microalloyed Al-Cu-Si-Ge alloy, plastic deformation prior to ageing at 160°C results in a faster hardening response and further increase in peak hardness, if the pre-deformation is below 15%. **Figure 1(c)** shows that a maximum peak hardness value of $H_v = 190$ is obtained for 8% pre-deformation. For 15% pre-deformation peak hardness is the same as that for the undeformed alloy ($H_v = 170$), but it is reached after 3 h, which is about six times faster than without pre-deformation. Further increasing pre-deformation to 30% prior to ageing results in a reduction of peak hardness. Thus, pre-deformation of about 8% is considered as an optimum to maximize peak hardness.

The results presented in this work clearly explain how the incorporation of Si and Ge microalloying elements combined with prior plastic deformation dramatically alters the hardening response with respect to that of the binary Al-Cu alloy. In Al-Cu, a peak hardness of $H_v = 134$ is obtained after 100 h ageing at 160°C whereas the combination of microalloying with Si and Ge and 8% pre-deformation increases peak hardness to $H_v = 190$ and reduces the time to peak ageing by a factor of 5, to 20 h. For 15% pre-deformation, the time to obtain peak hardness is reduced to 3 h, *i.e.* by a factor of about 30 with a peak hardness of $H_v = 170$, which is considerably higher than that of the binary alloy.

TEM characterization of the material deformed to 8% demonstrated that at peak ageing the microstructure is qualitatively similar to that without pre-deformation, containing θ'' disc shaped particles, rod-shaped Si-Ge precipitates and θ' plate shaped precipitates. However, as can be observed in **Table 3**, the PA microstructure in the Al-Cu-Si-Ge alloy after 8% pre-deformation displays larger diameter plates of θ' phase with a similar density when compared to the undeformed material, whereas the size and density of Si-Ge and θ'' precipitates is

almost unchanged by pre-deformation. This indicates that the increase in hardness of the material deformed to 8% can be attributed to the increased size of θ' precipitates.

It is worth noting that the largest difference in hardness between 8% pre-deformed and undeformed Al-Cu-Si-Ge specimens, is observed during the early stages of ageing. Microstructural characterization after 3 hours (Figure 4) presents a dense distribution of θ'' precipitates in both materials while the densities of Si-Ge and θ' precipitates are around 20 times lower than that of the θ'' precipitates. Detailed analysis of the microstructures reveal that the Si-Ge/ θ' precipitates are usually larger in the 8% pre-deformed specimen ($l_{\text{Si-Ge}} > 5$ nm, $l_{\theta'} > 10$ nm) than in the undeformed material ($l_{\text{Si-Ge}} < 5$ nm, $l_{\theta'} < 10$ nm). The under-aged microstructure after 10 hours ageing clearly shows that the θ' precipitates are much more developed in the 8% pre-deformed material compared to the undeformed material (Figure 5). In both alloys heterogeneous precipitation of θ' precipitates on Si-Ge precipitates is observed. Based on these results, it's possible to relate the faster development of θ' precipitates to the dislocations introduced by pre-deformation that provide fast diffusion paths for solute atoms. In summary, the faster increase of hardness in the material that has been pre-deformed to 8% is associated to the accelerated growth of θ' precipitates caused by enhanced solute diffusion along dislocation cores.

In the Al-Cu-Si-Ge alloy that has been pre-deformed to 15%, peak hardness is reached after ageing for 3 hours. The peak-aged microstructure qualitatively resembles that of the Al-Cu alloy pre-deformed to 8%, where a very high density of θ'' precipitates is observed among a low density of large θ' plates. However, the marked difference in peak hardness ($H_v = 170$ in Al-Cu-Si-Ge compared to $H_v = 130$ in Al-Cu) is associated with the contribution of heterogeneous nucleation of θ' plates at Si-Ge precipitates in the quaternary alloy. However, θ' plates that are not associated with Si-Ge precipitates are also observed indicating that as pre-deformation is increased, a fraction of θ' plates form by heterogeneous nucleation at dislocations. The faster evolution of the θ' plates in pre-deformed Al-Cu-Si-Ge as compared to the undeformed alloys is accounted for by enhanced diffusion along dislocation cores. In the overaged condition, θ' plates grow at the expense of θ'' precipitates.

The faster hardening kinetics and higher hardness values of the microalloyed and pre-deformed material as compared to binary Al-Cu, observed after pre-deformation to either 8% or 15%, are then related to the combination of heterogeneous nucleation of the θ' phase on Si-Ge precipitates and enhanced diffusion along dislocation cores.

For 30% pre-deformation, peak hardness occurs after very short aging times, but to a lower hardness value. Since θ' plates are observed and they are not associated to Si-Ge precipitates in the 15% pre-deformed alloy, it is suggested that as pre-deformation is increased, a progressively larger fraction of θ' plates nucleate on dislocations. The distribution of θ' plates nucleated on dislocations is less efficient in increasing hardness, as borne out by the results for the

binary Al-Cu alloy.

Finally, in the Al-Cu-Si-Ge alloy it has been observed that the over-aged condition is reached earlier as the degree of pre-deformation increases, indicating that deformation promotes coarsening. This effect can again be related to faster diffusion along dislocation cores.

5. Conclusions

The combined effect of microalloying with Si and Ge additions and pre-deformation on the hardening response at 160°C in Al-Cu has been thoroughly studied. The effects of pre-deformation on the hardening response in binary Al-Cu and ternary Al-Si-Ge have been also investigated for comparison. The main conclusions are as follows:

1) In Al-Si-Ge, pre-deformation results in a small shift of hardness to higher values, but does not alter the precipitation kinetics of Si-Ge precipitates.

2) In Al-Cu, prior deformation promotes the precipitation of the θ' phase, resulting in a shorter time to achieve peak hardness, but does not increase the peak hardness value.

3) In Al-Cu-Si-Ge, ageing at 160°C without pre-deformation results in higher peak hardness values and much shorter times to achieve peak hardness as in Al-Cu. Compared to previous results at 190°C, peak hardness is higher but the time to reach peak hardness is increased. TEM characterization shows a complex microstructure that includes a very high density of disc-shaped θ'' precipitates and lower densities of rod-shaped Si-Ge particles and plate-shaped θ' precipitates. The θ'' precipitates contribute significantly to peak hardness.

4) Pre-deformation to 8% prior to ageing at 160°C in microalloyed Al-Cu-Si-Ge further accelerated the hardening response and increased peak hardness. Higher amounts of pre-deformation result in reduced peak hardness and accelerate the onset to the overaged condition.

5) An optimum degree of pre-deformation that maximizes the hardening response is estimated to be about 8%.

6) TEM characterization of 8% pre-deformed Al-Cu-Si-Ge in the peak aged condition shows a qualitatively similar microstructure as that of the undeformed alloy. Precipitate densities are similar, but the θ' precipitates are larger. This effect is attributed to enhanced diffusion along dislocation cores. Overageing was associated with the coarsening of θ' phase plates at the expense of θ'' precipitates.

7) In the under-aged condition, the microstructure of both pre-deformed and undeformed specimens is dominated by a very high density of θ'' precipitates and the incipient formation of Si-Ge and θ' phase particles. Pre-deformation resulted in faster growth of the θ' phase and Si-Ge precipitates, particularly during the early stages of hardening, and is related to enhanced diffusion along dislocation cores.

Acknowledgements

This work was carried out under projects 2011-0643 and 2015-1641 sponsored

by the ANPCyT, PIP 11220110100513 sponsored by Conicet and 06/C330 Universidad Nacional de Cuyo. Dr. M.V. Castro Riglos acknowledges a Conicet fellowship for her PhD studies as this work was performed as part of her PhD Thesis. The authors also want to thank Mrs. M. Segura and Dr. J. Paul for their contribution to the improvement of this text.

References

- [1] Polmear, I.J. and St. John, D. (2005) Light Alloys: From Traditional Alloys to Nanocrystals. 4th Edition, Butterworth-Heinemann, London.
- [2] Hardy, H.K. (1951-1952) The Ageing Characteristics of Ternary Aluminium-Copper Alloys with Cadmium, Indium or Tin. *Journal of the Institute of Metals*, **80**, 483-492.
- [3] Hardy, H.K. (1950-1951) The Effect of Small Quantities of Cd, In, Sn, Sb, Tl, Pb or Bi on the Ageing Characteristics of Cast and Heat Treated Aluminium-4% Copper-0.15% Titanium Alloy. *Journal of the Institute of Metals*, **78**, 169-194.
- [4] Silcock, J.M., Heal, T.J. and Hardy, H.K. (1955) The Structural Ageing Characteristics of Ternary Aluminum-Copper Alloys with Cadmium, Indium, or Tin. *Journal of the Institute of Metals*, **84**, 23-31.
- [5] Ringer, S.P., Hono, K. and Sakurai, T. (1995) Nucleation and Growth of θ' Precipitation in Sn Modified Al-Cu Alloys: APFIM/TEM Observations. *Applied Surface Science*, **87/88**, 223-227. [https://doi.org/10.1016/0169-4332\(94\)00514-1](https://doi.org/10.1016/0169-4332(94)00514-1)
- [6] Polmear, I.J. (1964) The Effects of Small Additions of Silver on the Aging of Some Aluminium Alloys. *Transactions of the Metallurgical Society AIME*, **230**, 1331-1331.
- [7] Vietz, J.T. and Polmear, I.J. (1966) The Influence of Small Additions of Silver on the Ageing of Aluminium Alloys: Observations on Al-Cu-Mg Alloys. *Journal of the Institute of Metals*, **94**, 410-419.
- [8] Ringer, S.P., Sakurai, T. and Polmear, I.J. (1997) Origins of Hardening in Aged Al-Cu-Mg-(Ag) Alloys. *Acta Materialia*, **45**, 3731-3744. [https://doi.org/10.1016/S1359-6454\(97\)00039-6](https://doi.org/10.1016/S1359-6454(97)00039-6)
- [9] Chester, R.J. and Polmear, I.J. (1980) TEM Investigation of Precipitates in AlCuMgAg and AlCuMg Alloys. *Micron*, **11**, 311-312.
- [10] Knowles, K.M. and Stobbs, W.M. (1988) The Structure of {111} Age-Hardening Precipitates in Al-Cu-Mg-Ag Alloys. *Acta Crystallographica B*, **44**, 207-227. <https://doi.org/10.1107/S0108768187012308>
- [11] Muddle, B.C. and Polmear, I.J. (1989) The Precipitate Ω Phase in Al-Cu-Mg-Ag Alloys. *Acta Metallurgica*, **37**, 777-789. [https://doi.org/10.1016/0001-6160\(89\)90005-9](https://doi.org/10.1016/0001-6160(89)90005-9)
- [12] Chopra, H.D., Liu, K.J., Muddle, B.C. and Polmear, I.J. (1995) The Structure of Metastable {111} Precipitates in an Al-2.5 wt% Cu-1.5 wt% Mg-0.5 wt% Ag Alloy. *Philosophical Magazine Letters*, **71**, 319-324. <https://doi.org/10.1080/09500839508241014>
- [13] Macchi, C., Tolley, A., Giovachini, R., Polmear, I.J. and Somoza, A. (2015) Influence of a Microalloying Addition of Ag on the Precipitation Kinetics of an Al-Cu-Mg Alloy with High Mg:Cu Ratio. *Acta Materialia*, **98**, 275-287. <https://doi.org/10.1016/j.actamat.2015.07.032>
- [14] Mitlin, D., Radmilovic, V., Dahmen, U. and Morris Jr., J.W. (2001) Precipitation and Ageing in AlCuSiGe. *Metallurgical and Materials Transactions A*, **32**, 197-199.

- <https://doi.org/10.1007/s11661-998-0335-3>
- [15] Mitlin, D., Radmilovic, V., Morris Jr., J.W. and Dahmen, U. (2003) On the Influence of Si-Ge Additions on the Ageing Response of Al-Cu. *Metallurgical and Materials Transactions A*, **34**, 735-741.
- [16] Ferragut, R. and Somoza, A. (1999) Positron, Age-Hardening and Precipitation in Predeformed 2024 (Al-Cu-Mg) Alloy. *Physical Status Solidi A*, **175**, R1-R2. [https://doi.org/10.1002/\(SICI\)1521-396X\(199909\)175:1<R1::AID-PSSA99991>3.0.CO;2-3](https://doi.org/10.1002/(SICI)1521-396X(199909)175:1<R1::AID-PSSA99991>3.0.CO;2-3)
- [17] Tolley, A., Ferragut, R. and Somoza, A. (2009) Microstructural Characterization of a Commercial Al-Cu-Mg Alloy Combining Transmission Electron Microscopy and Positron Annihilation Spectroscopy. *Philosophical Magazine*, **89**, 1095-1110. <https://doi.org/10.1080/14786430902889674>
- [18] Hardy, H.K. (1954-55) Aluminium-Copper-Cadmium Sheet Alloys. *Journal of the Institute of Metals*, **83**, 337-346.
- [19] Castro Riglos, M.V., Taquire de la Cruz, M. and Tolley, A. (2011) Accelerated Age Hardening by Plastic Deformation in Al-Cu with Minor Additions of Si and Ge. *Scripta Materialia*, **64**, 169-172. <https://doi.org/10.1016/j.scriptamat.2010.09.036>
- [20] Kelly, P.M., Jostsons, A., Blake, R.G. and Napier, J.G. (1975) Determination of Foil Thickness by Scanning Transmission Electron Microscopy. *Physical Status Solidi A*, **31**, 771-780. <https://doi.org/10.1002/pssa.2210310251>
- [21] Mukhopadhyay, A.K. (2001) Influence of Cu Additions on the Morphology of GeSi Precipitates in an Al-Ge-Si Alloy. *Metallurgical and Materials Transactions A*, **32**, 1949-1958. <https://doi.org/10.1007/s11661-001-0007-z>